Strong nondipole effects in low-energy photoionization of the $5s$ and $5p$ subshells of xenon

W. R. Johnson
Department of Physics, University of Notre Dame, Notre Dame, Indiana 46556

K. T. Cheng
University of California, Lawrence Livermore National Laboratory, Livermore, California 94550
(Received 5 September 2000; published 8 January 2001)

Large nondipole effects are predicted in the angular distribution of photoelectrons from the $5s$ and $5p$ subshells of xenon for photon energies below 200 eV. The nondipole parameter γ_{5s} exhibits a dispersion-curve variation near the first minimum of the $5s$ cross section at 35 eV, reaching a minimum value of -0.8 near 40 eV. Rapid variation of γ_{5s} is also found near the second minimum of the $5s$ cross section at 150 eV, where γ_{5s} reaches a maximum value of 1.2. Smaller, but significant, nondipole effects are also found in the parameter $\zeta_{5p}=\gamma_{5p}+3\delta_{5p}$, which has a maximum value of 0.15 near 50 eV, and a second maximum value of 0.18 near 160 eV. The higher energy maxima in γ_{5s} and ζ_{5p} arise from correlation enhanced by shape resonances in the $4p\rightarrow f$ quadrupole photoionization channels. These predictions are based on relativistic random-phase approximation calculations in which excitations from $5p$, $5s$, $4d$, $4p$, and $4s$ subshells are coupled.

DOI: 10.1103/PhysRevA.63.022504 PACS number(s): 32.80.Fb, 31.25.Eb, 32.30.Rj

I. INTRODUCTION

We present results of relativistic random-phase approximation (RRPA) [1] calculations of photoionization of the outer $5s$ and $5p$ subshells of xenon. Partial cross sections $\sigma_{n\kappa}(\omega)$, angular-distribution asymmetry parameters $\beta_{n\kappa}(\omega)$, and nondipole parameters $\delta_{n\kappa}(\omega)$ and $\gamma_{n\kappa}(\omega)$ for $5s$ and $5p$ photoelectrons are given for photon energies ω below 200 eV. The RRPA calculations of the electric dipole (E1) amplitudes include the 20 possible dipole excitation channels of the $5p$, $5s$, $4d$, $4p$, and $4s$ subshells, while the electric quadrupole (E2) amplitudes include the 25 possible quadrupole excitation channels of these subshells. The present results for $\sigma_{n\kappa}(\omega)$ and $\beta_{n\kappa}(\omega)$ are in good agreement with the previous 13-channel RRPA calculations of Ref. [2] which include all E1 channels from the $5p$, $5s$, and $4d$ subshells. Results for the nondipole parameters $\gamma_{n\kappa}(\omega)$ and $\delta_{n\kappa}(\omega)$ are new; these nondipole parameters show interesting features, especially near the $4p$ ionization threshold.

Corrections to the dipole angular distribution arising from dipole-quadrupole interference were considered two decades ago by Amusia and Cherepkov [3], who gave formulas for dipole-quadrupole interference contributions to the photoionization differential cross section. In recent years, theoretical investigations of nondipole corrections have been undertaken by Bechler and Pratt [4], who studied dipole-quadrupole interference effects on the photoelectron angular distribution for $1s$, $2s$, and $2p$ shells of elements with nuclear charges Z ranging from 6 to 40 in the Coulomb field and screened Coulomb-field approximations, by Scofield [5], who gave general formulas for the interference contributions to the differential cross section and carried out calculations using Dirac-Slater central potentials, and by Cooper [6], who evaluated the dipole-quadrupole interference corrections nonrelativistically for noble-gas atoms using Herman-Skillman potentials. Recently, Amusia *et al.* [7] carried out Hartree-Fock (HF) and random-phase approximation (RPAE) calculations of the nondipole parameter γ_{ns} for the $1s$ and $3s$ subshells of argon at low energies and found large nondipole effects near threshold.

Measurements of the nondipole angular-distribution parameters for inner shells of Ar and Kr were reported in Refs. [8] and [9] and found to be in excellent agreement with independent-particle approximation (IPA) calculations. However, measurements of nondipole effects for the $2p$ subshells of Ne reported in [10] were systematically higher than the IPA predictions for energies above the Ne $1s$ threshold at 870 eV. In Ref. [11], random-phase approximation calculations were carried out to investigate the possible influence of correlation on the nondipole parameters. These calculations confirmed a large intershell coupling effect on the dipole parameter β_{2p} observed experimentally, but failed to explain the substantial differences between IPA calculations and experiment for the nondipole parameter $\zeta_{2p}=\gamma_{2p}+3\delta_{2p}$ at such high energies. The problem was finally resolved by Derevianko *et al.* [12], who show that these discrepancies actually arise from octupole-dipole and quadrupole-quadrupole interferences.

In the present work, the RRPA is applied to study nondipole effects in the photoionization of the $n=5$ shell of xenon for photon energies below 200 eV. For such low energies, octupole-dipole and quadrupole-quadrupole interferences are insignificant, but correlation effects are known to be important. Large nondipole modifications of the $5s$ photoelectron angular distribution are found in this energy range and smaller, but significant, nondipole effects are found for the $5p$ angular distribution. The energy-dependence of the nondipole angular distribution parameters near threshold are similar to those predicted in recent IPA calculations [13], but are found to be very sensitive to intershell correlation. In particular, coupling of the $5s$ and $5p$ subshells to the $4d$ subshell changes the behavior of nondipole parameters from that predicted by IPA calculations substantially. In general, $4p$ correlation has negligible effects on the partial cross sec-

tions $\sigma_{n\kappa}$ and the angular distribution asymmetry parameters $\beta_{n\kappa}$, but modifies the nondipole parameters $\gamma_{n\kappa}$ and $\delta_{n\kappa}$ significantly near the $4p$ thresholds at $\omega \sim 160$ eV. We shall show that these enhanced nondipole effects are due to the presence of shape resonances in the $4p \rightarrow f$ quadrupole photoionization channels. The effect of $4s$ correlation is completely negligible in this energy range.

II. RESULTS AND DISCUSSIONS

A detailed analysis of the dipole and nondipole angular distribution parameters suitable for relativistic calculations was presented in [13] and we follow the notation of that paper here. The differential cross section for photoionization of an electron from a subshell $n\kappa$ of a closed-shell atom is

$$\frac{d\sigma_{n\kappa}}{d\Omega} = \frac{\sigma_{n\kappa}(\omega)}{4\pi}\{1 + \beta_{n\kappa}(\omega) P_2(\cos\theta) + [\delta_{n\kappa}(\omega) + \gamma_{n\kappa}(\omega)\cos^2\theta]\sin\theta\cos\phi\},$$

where θ and ϕ are polar coordinates of the photoelectron momentum vector $\boldsymbol{p}$ in a coordinate system with the photon polarization vector $\boldsymbol{\varepsilon}$ oriented along the z axis and the photon propagation vector $\boldsymbol{k}$ oriented along the x axis. The angular distribution asymmetry parameter $\beta_{n\kappa}(\omega)$ results from interferences between E1 amplitudes, while the nondipole parameters $\delta_{n\kappa}(\omega)$ and $\gamma_{n\kappa}(\omega)$ result from interferences between E1 and E2 amplitudes. Since measurements of the nondipole parameter are often carried out at the magic angle where $\cos^2\theta = 1/3$, it is convenient to introduce a third parameter $\zeta_{n\kappa}(\omega) = \gamma_{n\kappa}(\omega) + 3\,\delta_{n\kappa}(\omega)$. For ns subshells, $\delta_{ns}(\omega) \equiv 0$ and $\zeta_{ns}(\omega) \equiv \gamma_{ns}(\omega)$.

Our results for the xenon photoionization parameters are presented in Figs. 1 and 2. In these figures, we show results of a sequence of RRPA calculations of increasing complexity over the entire photon energy range from the first $5p$ threshold to 200 eV. Our starting point for studies of photoionization of the $5s$ subshell is a two-channel calculation in which only $5s \rightarrow p_{1/2}$ and $5s \rightarrow p_{3/2}$ excitations are included. These calculations are labeled ''$5s$ only'' in Fig. 1. For photoionization of the $5p$ subshell, our starting point is a five-channel calculation in which the two $5p \rightarrow s$ and three $5p \rightarrow d$ channels are included; these calculations are labeled ''$5p$ only'' in Fig. 2. At the next level of sophistication, we show results from ''$5s+5p$'' calculations in which excitations of the seven $5s$ and $5p$ excitation channels are coupled. Next, we show results from more realistic 13-channel ''$5s+5p+4d$'' calculations in which excitations of the $4d$ subshell are included; and, finally, we show results of the 20-channel ''$5s+5p+4d+4p+4s$'' calculations in which excitations of the $4s$ and $4p$ subshells are also included. In each case, corresponding E2 photoionization calculations are also carried out. They include up to 25 quadrupole channels from the $n=4$ and 5 subshells.

All calculations predict a Cooper minimum in σ_{5s} near the $5s$ threshold. The exact location of this minimum changes as we increase the number of excitation channels, but stabilizes after the $4d$ excitations are added. Moreover,

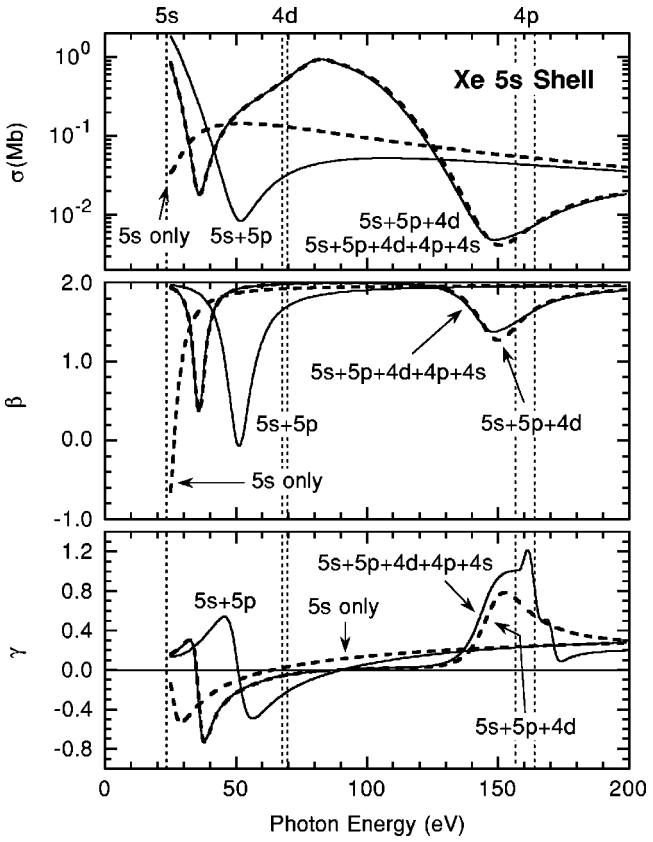

FIG. 1. Photoionization parameters for the $5s$ subshell of xenon. Vertical dotted lines are experimental subshell thresholds.

when excitations of the $4d$ subshell are included in the calculation, a second minimum appears in the $5s$ cross section at 150 eV. Similarly, $4d$ correlation leads to the appearance of two minima in σ_{5p} near 50 and 160 eV, respectively. Only the first minimum in σ_{5s} shows up in uncoupled IPA calculations; the other three minima in σ_{5s} and σ_{5p} are results of couplings with the ''giant resonance'' in the $4d \rightarrow f$ excitation channels [14]. Although $4d$ correlation leads to substantial modifications of partial cross sections σ_{5s} and σ_{5p} and in the angular distribution parameters β_{5s} and β_{5p}, the influence of the $4p$ and $4s$ excitations on these four parameters is insignificant. Consequently, the cross sections and β parameters for the $5s$ and $5p$ shells obtained here, which include excitations from $5s$, $5p$, $4d$, $4p$, and $4s$ subshells, are in close agreement with previous calculations of Ref. [2], in which $5s$, $5p$, and $4d$ excitations were included, but $4s$ and $4p$ excitation channels were ignored.

Turning now to the nondipole parameter γ_{5s} shown in the lower panel of Fig. 1, we note that near the first Cooper minimum in the $5s$ partial cross section at 35 eV, γ_{5s} has a dispersion-curve shape which, like the corresponding dip in the β_{5s} curve, is strongly modified by channel couplings. In particular, γ_{5s} reaches a minimum value of -0.8 at 40 eV in calculations including excitations of the $4d$ subshell. This unusually large nondipole effect at such low energies is clearly enhanced by the presence of the Cooper minumum where the E1 amplitudes are suppressed, resulting in larger E1-E2 interference effects. We mention in passing that the

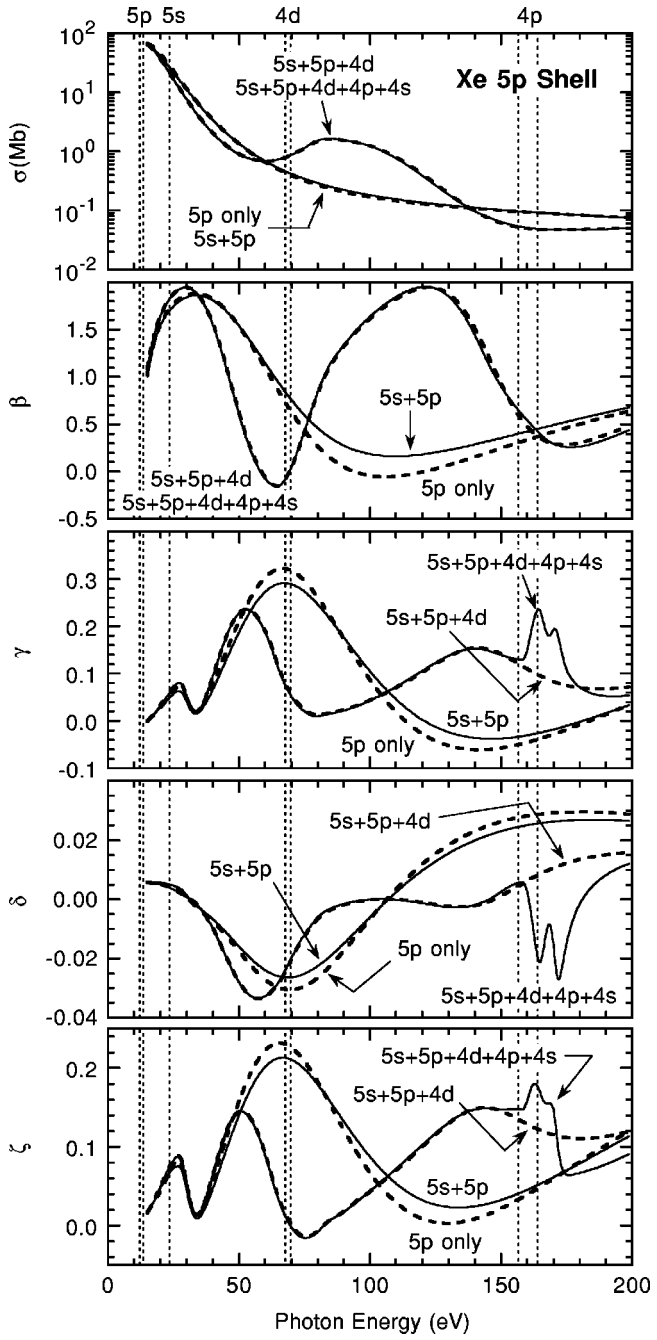

FIG. 2. Photoionization parameters for the $5p$ subshell of xenon. Vertical dotted lines are experimental subshell thresholds.

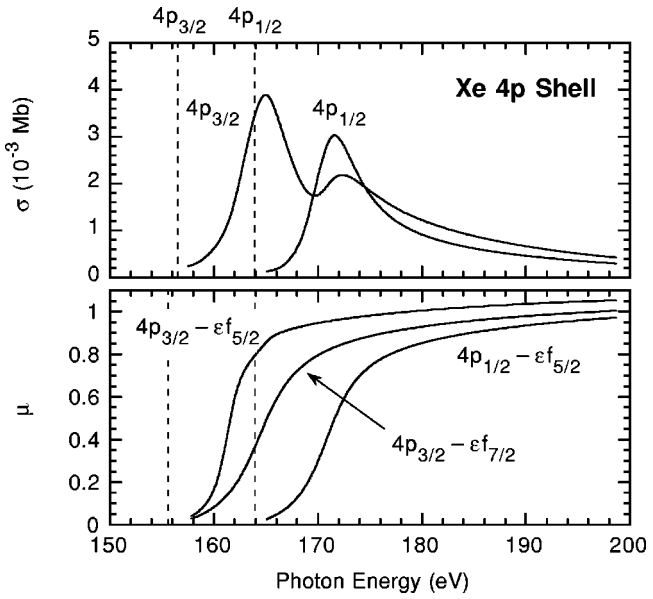

FIG. 3. The $4p \rightarrow f$ quadrupole shape resonances in xenon. Vertical dotted lines are experimental subshell thresholds.

experimental values of β_{5s} in this energy range as reported in Refs. [15] and [16] were obtained assuming a pure dipole form for the angular distribution where $\gamma_{5s}=\delta_{5s}=0$.

At higher energies, γ_{5s} remains close to zero until the second cross-section minimum at 150 eV is reached. There, γ_{5s} becomes large again in calculations that include $4d$ excitation channels. It is interesting to note that while the low-energy part of γ_{5s} remains unchanged when $4p$ and $4s$ excitation channels are included, the γ_{5s} curve near the $4p$ thresholds is greatly influenced by the $4p$ channels. In particular, the peak value of γ_{5s} increases from 0.8 in the $5s+5p+4d$ calculations to 1.2 in the $5s+5p+4d+4p+4s$ calculations. We return to this point later.

The nondipole parameters γ_{5p}, δ_{5p}, and ζ_{5p} shown in the three lower panels of Fig. 2 also have interesting features. We note first that the size of δ_{5p} is very small throughout the entire energy range. As a result, the γ_{5p} and ζ_{5p} curves in Fig. 2 are similar. Two successive maxima in γ_{5p} and ζ_{5p} appear in the interval 20–70 eV, where the $5p$ cross section is large. When the $4d$ channels are included, the second of these low-energy maxima shifts down to 50 eV and are substantially reduced, while new maxima appear near 140 eV. As in the case of γ_{5s}, the inclusion of additional $4p$ and $4s$ channels has very little effect on these nondipole parameters at low energy, but leads to unexpectedly strong, double-peak, resonancelike features near the $4p$ threshold at 160 eV. These features are due mainly to $4p$ channel coupling, as $4s$ correlation effects are found to be quite negligible. The fact that these resonancelike features only show up in the nondipole parameters near the $4p$ threshold for both the $5s$ and $5p$ shells suggests that they come from the E2 amplitudes which, apparently, are strongly influenced by coupling with the $4p$ quadrupole excitation channels in this energy range. Closer inspections show that these localized E2 correlation enhancements are due to shape resonances in the $4p \rightarrow f$ quadrupole excitation channels which appear just above the $4p_{3/2}$ and $4p_{1/2}$ thresholds.

In Fig. 3 these shape resonances are examined in greater detail. In the upper panel of this figure, the E2 partial cross sections from the $4p_{1/2}$ and $4p_{3/2}$ shells are shown. They clearly look like ''giant resonances'' extending well over 10 eV above the two $4p$ thresholds. In the lower panel of Fig. 3, the quantum defects of the outgoing f partial waves in each of the three excitation channels are plotted. These f-wave quantum defects μ are seen to change by 1 (the corresponding phase shifts $\delta=\pi\mu$ change by π) in the same energy range, indicating that these are indeed shape resonances in the quadrupole excitation channels. These ''giant quadrupole

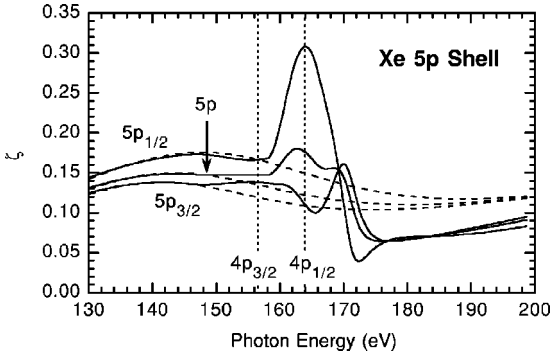

FIG. 4. Nondipole parameter $\zeta_{5p_j}=\gamma_{5p_j}+3\delta_{5p_j}$ for the $5p_{1/2}$ and $5p_{3/2}$ subshells of xenon in the vicinity of the $4p_{1/2}$ and $4p_{3/2}$ thresholds. Solid lines: $5s+5p+4d+4p+4s$ calculations. Dashed lines: $5s+5p+4d$ calculations. Vertical dotted lines are experimental subshell thresholds.

resonances'' boost the E2 photoionization amplitudes of the $5s$ and $5p$ shell through quadrupole channel coupling. Along with the reduced E1 amplitudes in the vicinity of dipole cross section minima near the $4p$ threshold, nondipole effects in photoionization of the $5s$ and $5p$ shells are thus greatly enhanced. It should be noted that there are similar shape resonances in the $5p\rightarrow f$ quandrupole excitation channels just above the $5p$ threshold at 13 eV. But since the $5p$ cross section is close to 100 Mb there, no enhancement in the nondipole parameters from those shape resonances can be seen.

The $5p$ photoionization parameters are weighted sums of parameters for the individual $5p_{1/2}$ and $5p_{3/2}$ photoelectrons. Thus, for example,

$$\zeta_{5p}(\omega)=\frac{\sigma_{5p_{1/2}}(\omega)\zeta_{5p_{1/2}}(\omega)+\sigma_{5p_{3/2}}(\omega)\zeta_{5p_{3/2}}(\omega)}{\sigma_{5p_{1/2}}(\omega)+\sigma_{5p_{3/2}}(\omega)}.$$

In general, the $5p_{1/2}$ and $5p_{3/2}$ photoionization parameters are similar to the weighted averages shown in Fig. 2. Near the $4p$ threshold, however, resonant enhancement leads to very different $5p_{1/2}$ and $5p_{3/2}$ nondipole parameters. In Fig. 4 we show the individual contributions $\zeta_{5p_{1/2}}(\omega)$, $\zeta_{5p_{3/2}}(\omega)$, and $\zeta_{5p}(\omega)$ at higher resolution in the vicinity of the $4p_j$ thresholds. The presence of $4p_j\rightarrow ns$ and $4p_j\rightarrow nd$ autoionization resonances complicates the behavior from below the $4p_{3/2}$ threshold to the $4p_{1/2}$ threshold ($\omega\sim 150$–164 eV); we average over these resonances in the figure. Results obtained without the $4p$ and $4s$ excitation channels are also shown as dashed lines in Fig. 4. It is interesting to note that the resonances in the individual parameters $\zeta_{5p_{1/2}}(\omega)$ and $\zeta_{5p_{3/2}}(\omega)$ are slightly out of phase. As a result, the size of the composite parameter $\zeta_{5p}(\omega)$ is substantially reduced.

In summary, we find that the nondipole photoionization parameter γ_{5s} for the $5s$ subshell of xenon has a dispersion-shaped dependence on energy near 50 eV reaching a minimum of -0.8, and a resonant behavior near 160 eV reaching a maximum of 1.2. The nondipole parameter $\zeta_{5p}(\omega)$ also reaches a local maximum of 0.15 near 50 eV and a second maximum of 0.18 near 160 eV. The high-energy maxima in γ_{5s} and ζ_{5p} near the $4p$ threshold are associated with shape resonances in the $4p\rightarrow f$ quadrupole excitation channels.

ACKNOWLEDGMENTS

The work of W.R.J. was supported in part by NSF Grant No. Phy 99-70666. The work of K.T.C. was performed under the auspices of the U. S. Department of Energy by the University of California, Lawrence Livermore National Laboratory under Contract No. W-7405-ENG-48.

[1] W.R. Johnson and C.D. Lin, Phys. Rev. A **20**, 964 (1979); W.R. Johnson and K.T. Cheng, *ibid.* **20**, 978 (1979).
[2] K.-N. Huang, W.R. Johnson, and K.T. Cheng, At. Data Nucl. Data Tables **26**, 33 (1981).
[3] M. Ya. Amusia and N. A. Cherepkov, *Case Studies in Atomic Physics* (North-Holland, Amsterdam, 1975), Vol. 5, p. 155.
[4] A. Bechler and R.H. Pratt, Phys. Rev. A **39**, 1774 (1989); **42**, 6400 (1990).
[5] J.H. Scofield, Phys. Rev. A **40**, 3054 (1989); Phys. Scr. **41**, 59 (1990).
[6] J.W. Cooper, Phys. Rev. A **42**, 6942 (1990); **47**, 1841 (1993).
[7] M. Ya Amusia, A.S. Baltenkov, Z. Felfli, and A.Z. Msezane, Phys. Rev. A **59**, R2544 (1999).
[8] B. Krässig, M. Jung, D.S. Gemmell, E.P. Kanter, T. LeBrun, S.H. Southworth, and L. Young, Phys. Rev. Lett. **75**, 4736 (1995).
[9] M. Jung, B. Krässig, D.S. Gemmell, E.P. Kanter, T. LeBrun, S.H. Southworth, and L. Young, Phys. Rev. A **54**, 2127 (1996).
[10] O. Hemmers, G. Fischer, P. Glans, D.L. Hansen, H. Wang, S.B. Whitfield, R. Wehlitz, J.C. Levin, I.A. Sellin, R.C.C. Perea, E.W.B. Dias, H.S. Chakraborty, P.C. Deshmukh, S.T. Manson, and D.W. Lindle, J. Phys. B **30**, L727 (1997).
[11] W.R. Johnson, A. Derevianko, K.T. Cheng, V.K. Dolmatov, and S.T. Manson, Phys. Rev. A **59**, 3609 (1999).
[12] A. Derevianko, O. Hemmers, S. Oblad, P. Glans, H. Wang, S.B. Whitfield, R. Wehlitz, I.A. Sellin, W.R. Johnson, and D.W. Lindle, Phys. Rev. Lett. **84**, 2116 (2000).
[13] A. Derevianko, W.R. Johnson, and K.T. Cheng, At. Data Nucl. Data Tables **73**, 153 (1999).
[14] K.T. Cheng and W.R. Johnson, Phys. Rev. A **28**, 2820 (1983).
[15] A. Fahlman, T.A. Carlson, and M.O. Krause, Phys. Rev. Lett. **50**, 1114 (1983).
[16] H. Derenbach and V. Schmidt, J. Phys. B **16**, L337 (1983).